Available online at www.elixirpublishers.com (Elixir International Journal)

Applied Mathematics

Elixir Appl. Math. 51 (2012) 10794-10801

ISSN: 2229-712X

Magnetohydrodynamic free convective viscoelastic flow past a vertical cone with variable heat and mass flux In non-darcian porous media

S. Gouse Mohiddin[1,*], O. Anwar Beg[2] and S. Vijaya Kumar Varma[3]

[1]Department of Mathematics, Madanapalle Institute of Technology & Science, Madanapalle – 517325, AP, India.

[2]Biomechanics and Biotechnology Research, Aerospace Engineering Program, Mechanical Engineering Subject Group, Sheaf Building, Sheffield Hallam University, Sheffield, S1 1WB, England, UK.

[3]Department of Mathematics, Sri Venkateswara University, Tirupati – 517502.

ARTICLE INFO

Article history:

Received: 10 August 2012;

Received in revised form:

20 September 2012;

Accepted: 4 October 2012;

Keywords

Cone,

Non-Darcian porous media,

Finite difference method

Heat mass flux.

ABSTRACT

A numerical study of viscoelastic buoyancy-driven unsteady natural convection boundary layer flow past a vertical cone embedded in a non-Darcian isotropic porous regime with transverse magnetic field applied normal to the surface is considered. The heat and mass flux at the surface of the cone is modeled as a power-law according to $q_w(x) = x^m$ and $q_w^*(x) = x^n$ respectively, where x denotes the coordinate along the slant face of the cone. Both Darcian drag and Forchheimer quadratic porous impedance are incorporated into the two-dimensional viscous flow model. The transient boundary layer equations are then non-dimensionalized and solved by the Crank-Nicolson implicit difference method. The velocity, temperature and concentration fields have been studied for the effect of Grashof number, Darcy number, Forchheimer number, Prandtl number, surface heat flux power-law exponent (m), surface mass flux power-law exponent (n), Schmidt number, buoyancy ratio parameter and semi-vertical angle of the cone. Present results for selected variables for the purely fluid regime are compared with the non-porous study by Hossain and Paul [9] and are found to be in excellent agreement. The local skin friction, Nusselt number and Sherwood number are also analyzed graphically. The study finds important applications in geophysical heat transfer, industrial manufacturing processes and hybrid solar energy systems.

Introduction

Viscoelastic flows and transport phenomena arise in numerous areas of chemical, industrial process, biosystems, food processing and biomedical engineering. These include the rheology of liquid crystal precursors employed in the manufacture of carbon super-fibers, crude oil emulsion processing, paper coating rheological processing, propulsive ciliary transport of respiratory airway mucus, thermocapillary bubble dynamics in weakly elastic fluids, rheo-reactor phosphatation flows, flour rheology, mayonnaise elastico-viscous flows, xanthan gum hydrogel flows, polygalacturonase-based food stuff. Recently Prasad et al [14] studied the transient dissipative radiation free convection heat and mass transfer from a non-isothermal cone with variable surface conditions. Unsteady free convective heat and mass transfer in a walters-b viscoelastic flow along a vertical cone was presented in Gouse Mohiddin et al [7].

Combined heat and mass transfer in fluid-saturated porous media finds applications in a variety of engineering processes such as heat exchanger devices, petroleum reservoirs, chemical catalytic reactors and processes and others. A thorough discussion of these and other applications is available in the monographs by Ingham and Pop [11] and Nield and Bejan [13]. Comprehensive reviews of the much of the work communicated in porous media transport phenomena have been presented by Vafai [17] and Trevisan and Bejan [15]. Most studies dealing with porous media have employed the Darcy law. However, for high velocity flow situations, the Darcy law is inapplicable, since it does not account for inertial effects in the porous medium. Such flows can arise for example in the near-wellbore region of high capacity gas and condensate petroleum reservoirs and also in highly porous filtration systems under high blowing rates. The most popular approach for simulating high-velocity transport in porous media is the Darcy–Forchheimer drag force model. This adds a second-order (quadratic) drag force to the momentum transport equation. This term is related to the geometrical features of the porous medium and is independent of viscosity. Vafai and Tien [16] presented a seminal study discussing the influence of Forchheimer inertial effects in porous media convection. Chen and Chen [4] studied the mixed convective boundary layer flow from a vertical surface in a fluid-saturated non-Darcian porous medium including Forchheimer inertial effects. Hossain and Paul [10] studied thermal convection boundary layer flow with buoyancy and suction/blowing effects from a cone with non-uniform surface temperature. They extended this study [9] to consider non-uniform surface heat flux, both studies employing numerical methods. Chamkha et al. [3] studied the double-diffusive convection heat and mass transfer over a cone (and wedge) in Darcy-Forchheimer porous media. Magnetohydrodynamic (MHD) flow and heat transfer is of considerable interest because it can occur in many geothermal, geophysical,

Tele:

E-mail addresses: gousemaths@gmail.com

technological, and engineering applications such as nuclear reactors and others. The geothermal gases are electrically conducting and are affected by the presence of a magnetic field. Vajravelu and Nayfeh[18] studied hydromagnetic convection from a cone and a wedge with variable surface temperature and internal heat generation or absorption. Thusfar the transient thermal convection flow over a cone in Darcy-Forchheimer porous media has not been studied in the literature despite important applications in geothermics, geophysics and materials processing.

Constitutive Equations For The Walters-B Viscoelastic Model

$$p_{ik} = -pg_{ik} + p^*_{ik} \tag{i}$$

$$p^*_{ik} = 2\int_{-\infty}^{t} \Psi\left(t-t^*\right) e^{(1)}_{ik}(t^*)dt^* \tag{ii}$$

$$\Psi\left(t-t*\right) = \int_0^{\infty} \frac{N(\tau)}{\tau} e^{\left(-\left(t-t^*\right)/\tau\right)} d\tau \tag{iii}$$

where p_{ik} is the stress tensor, p is arbitrary isotropic pressure, g_{ik} is the metric tensor of a fixed coordinate system x_i, $e^{(1)}_{ik}$ is the rate of strain tensor and $N(\tau)$ is the distribution function of relaxation times, τ. The following generalized form of (ii) has been shown in [19] to be valid for all classes of motion and stress.

$$p^{*ik}(x,t) = 2\int_{-\infty}^{t} \Psi\left(t-t^*\right) \frac{\partial x^i}{\partial x^{*m}} \frac{\partial x^k}{\partial x^{*r}} e^{(1)mr}\left(x^* t^*\right) dt^* \tag{iv}$$

in which $x^*_i = x^*_i(x,t,t^*)$ denotes the position at time t^* of the element which is instantaneously at the position, x_i, at time, t. Liquids obeying the relations (i) and (iv) are of the Walters-B' type. For such fluids with short memory i.e. low relaxation times, equation (iv) may be simplified to:

$$p^{*ik}(x,t) = 2\eta_0 e^{(1)ik} - 2k_0 \frac{\partial e^{(1)ik}}{\partial t} \tag{v}$$

$$\eta_0 = \int_0^{\infty} N(\tau)d\tau$$

in which defines the limiting Walters-B'

$$k_0 = \int_0^{\infty} \tau N(\tau)d\tau$$

viscosity at low shear rates, is the Walters-B' viscoelasticity parameter and $\frac{\partial}{\partial t}$ is the convected time derivative. This rheological model is very versatile and robust and provides a relatively simple mathematical formulation which is easily incorporated into boundary layer theory for engineering applications

Mathematical Model

An axisymmetric unsteady natural convection boundary layer viscoelastic flow past a vertical cone with transverse magnetic field applied normal to the surface with variable heat and mass flux in a Darcy-Forchheimer fluid saturated porous medium in a cartesian (x, y) coordinate system is formulated mathematically in this section. Initially, it is assumed that the cone surface and the surrounding fluid which are at rest possess the same temperature T'_∞ and concentration level C'_∞ everywhere in the fluid. At time $t' > 0$, heat supplied from the cone surface to the fluid, concentration level near the cone surface are raised at a rate of $q_w(x) = x^m$ and $q^*_w(x) = x^n$ respectively, and they are maintained at the same level. It is assumed that the concentration C' of the diffusing species in the binary mixture is very less in comparison to the other chemical species, which are present and hence the Soret and Dufour effects are negligible. We consider viscous flow where pressure work, viscous dissipation and thermal dispersion effects are neglected. The coordinate system chosen (as shown in Fig.1) is such that the x-direction is measured along the cone surface from the leading edge O, and the y-direction is normal to the cone generator. The cone apex is located at the origin(x=y=0).

Here ϕ designates the semi-vertical angle of the cone and r is the local radius of the cone.

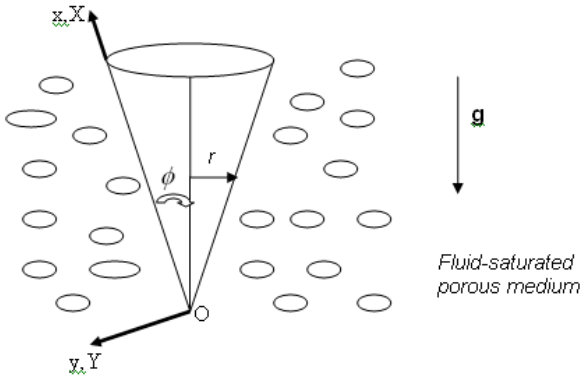

Figure 1: Physical Model

Then under the above assumptions, the governing boundary layer equations with Boussinesq's approximation are

$$\frac{\partial(ur)}{\partial x} + \frac{\partial(vr)}{\partial y} = 0 \tag{1}$$

$$\frac{\partial u}{\partial t'} + u\frac{\partial u}{\partial x} + v\frac{\partial u}{\partial y} = \nu\frac{\partial^2 u}{\partial y^2} - \frac{\sigma B_0^2}{\rho}u - k_0\frac{\partial^3 u}{\partial y^2 \partial t'} + g\beta\cos\phi(T'-T'_\infty) + g\beta^*\cos\phi(C'-C'_\infty) - \frac{\nu}{K}u - \frac{b}{K}u^2 \tag{2}$$

$$\frac{\partial T'}{\partial t'} + u\frac{\partial T'}{\partial x} + v\frac{\partial T'}{\partial y} = \alpha\frac{\partial^2 T'}{\partial y^2} \tag{3}$$

$$\frac{\partial C'}{\partial t'} + u\frac{\partial C'}{\partial x} + v\frac{\partial C'}{\partial y} = D\frac{\partial^2 C'}{\partial y^2} \tag{4}$$

where all terms are defined in the nomenclature. Under the Boussinesq approximation buoyancy effects are simulated only in the momentum equation, which is coupled to the energy equation, constituting a free convection regime. The corresponding spatial and temporal initial and boundary conditions at the surface and far from the cone take the form:

$$t' \le 0 : u = 0, v = 0, T' = T'_\infty, C' = C'_\infty \quad \text{for all x, y,}$$

$$t' > 0 : u = 0, v = 0, \frac{\partial T'}{\partial y} = -\frac{q_w(x)}{k}, \frac{\partial C'}{\partial y} = -\frac{q^*_w(x)}{D} \quad \text{at y = 0,}$$

$$u = 0, T' = T'_\infty, C' = C'_\infty \quad \text{at x = 0,} \qquad (5)$$
$$u \to 0, T' \to T'_\infty, C' \to C'_\infty \quad \text{as. } y \to \infty$$

where all the parameters defined in the nomenclature.

The equations (1) to (4) are highly coupled, parabolic and nonlinear. An analytical solution is clearly intractable and in order to facilitate a numerical solution we *non-dimensionalize* the model. Proceeding with the analysis we now introduce the following transformations:

$$X = \frac{x}{L}, \qquad Y = \frac{y}{L}(Gr_L)^{\frac{1}{4}}, \qquad R = \frac{r}{L}, \text{where}$$
$$r = x\sin\phi,$$
$$V = \frac{vL}{\nu}(Gr_L)^{\frac{-1}{4}}, \qquad U = \frac{uL}{\nu}(Gr_L)^{\frac{-1}{2}}, \quad t = \frac{\nu t'}{L^2}(Gr_L)^{\frac{1}{2}}$$
$$M = \frac{\sigma B_0^2 L^2}{\mu} Gr_L^{\frac{-1}{2}} \qquad (6)$$
$$T = \frac{T' - T'_\infty}{[q_w(L)L/k]}, \qquad Gr_L = \frac{g\beta\cos\phi[q_w L/k]L^4}{\nu^2},$$
$$\Pr = \frac{\nu}{\alpha}, \quad Da = \frac{K}{L^2}$$
$$C = \frac{C' - C'_\infty}{[q^*_w(L)L/D]}, \qquad \Gamma = \frac{k_0 Gr_L^{\frac{1}{2}}}{L^2},$$
$$N = \frac{\beta^*(C'_w - C'_\infty)}{\beta(T'_w - T'_\infty)}, \qquad Sc = \frac{\nu}{D}, \quad Fs = \frac{b}{L}$$

The transport equations (1) to (4) are thereby reduced to the following dimensionless form

$$\frac{\partial(UR)}{\partial X} + \frac{\partial(VR)}{\partial Y} = 0 \qquad (7)$$

$$\frac{\partial U}{\partial t} + U\frac{\partial U}{\partial X} + V\frac{\partial U}{\partial Y} = \frac{\partial^2 U}{\partial Y^2} - MU - \Gamma\frac{\partial^3 U}{\partial Y^2 \partial t} + T\cos\phi + NC\cos\phi - \frac{U}{DaGr_L} - \frac{Fs}{Da}U^2 \qquad (8)$$

$$\frac{\partial T}{\partial t} + U\frac{\partial T}{\partial X} + V\frac{\partial T}{\partial Y} = \frac{1}{\Pr}\frac{\partial^2 T}{\partial Y^2} \qquad (9)$$

$$\frac{\partial C}{\partial t} + U\frac{\partial C}{\partial X} + V\frac{\partial C}{\partial Y} = \frac{1}{Sc}\frac{\partial^2 C}{\partial Y^2} \qquad (10)$$

The corresponding non-dimensional initial and boundary conditions are given by

$$t \le 0 : U = 0, V = 0, T = 0, C = 0 \quad \text{for all X, Y,}$$
$$t > 0 : U = 0, V = 0, \frac{\partial T}{\partial Y} = -X^m, \frac{\partial C}{\partial Y} = -X^n \quad \text{at Y = 0,} \qquad (11)$$
$$U = 0, \quad T = 0, \quad C = 0 \quad \text{at X = 0,}$$
$$U \to 0, \quad T \to 0, \quad C \to 0 \quad \text{as } Y \to \infty.$$

Where again all the parameters are given in the nomenclature. The dimensionless local values of the skin friction, Nusselt number and the Sherwood number are given by the following expressions

$$\tau_x = -\left(\frac{\partial U}{\partial Y}\right)_{Y=0} \qquad (12)$$
$$Nu_x = -X\left(\frac{\partial T}{\partial Y}\right)_{Y=0} \qquad (13)$$
$$Sh_x = -X\left(\frac{\partial C}{\partial Y}\right)_{Y=0} \qquad (14)$$

Numerical Solution

In order to solve the unsteady, non-linear, coupled equations (7) – (10) under the conditions (11), an implicit finite difference scheme of Crank-Nicolson type has been employed which is discussed by many authors [1], [6], [7] and [12]. The finite difference scheme of dimensionless governing equations is reduced to tri-diagonal system of equations and is solved by Thomas algorithm as discussed in Carnahan et al. [2]. The region of integration is considered as a rectangle with $X_{\max} = 1$ and $Y_{\max} = 22$ where $Y_{\max}$ corresponds to $Y = \infty$ which lies very well out side both the momentum and thermal boundary layers. The maximum of Y was chosen as 22, after some preliminary investigation so that the last two boundary conditions of (11) are satisfied within the tolerance limit 10^{-5}. The mesh sizes have been fixed as $\Delta X = 0.05, \Delta Y = 0.05$ with time step $\Delta t = 0.01$. The computations are carried out first by reducing the spatial mesh sizes by 50% in one direction, and later in both directions by 50%. The results are compared. It is observed in all cases, that the results differ only in the fifth decimal place. Hence, the choice of the mesh sizes seems to be appropriate. The scheme is unconditionally stable. The local truncation error is $O(\Delta t^2 + \Delta Y^2 + \Delta X)$ and it tends to zero as $\Delta t, \Delta X$ and ΔY tend to zero. Hence, the scheme is compatible. Stability and compatibility ensure the convergence. The derivatives involved in Equations (12) – (14) are evaluated using five point approximation formula.

Results And Discussion

Only selective figures have been reproduced here for brevity. In the numerical computations the following values for the dimensionless thermophysical parameters are prescribed: viscoelasticity parameter (Γ) = 0.005, magnetic parameter (M) = 1.0, Grashof number (Gr_L) = 1.0, Darcy number (Da) = 0.1 (high permeability), Forchheimer number (Fs) = 0.1 (weak quadratic drag), Prandtl number (Pr) = 7.0 (water), Schmidt number (Sc) = 0.6 (oxygen diffusing in air), surface heat flux power law exponent (m) = 0.5, surface mass flux power law exponent (n) = 0.5, buoyancy ratio parameter (N) = 1.0 and semi-vertical angle of the cone (ϕ) = 20^0. All graphs therefore correspond to these values unless otherwise indicated. To test the accuracy of the computations the local shear stress and local Nusselt number computations for the non-porous case are compared with those of Hossain and Paul [9] for a heat flux gradient of m = 0.5 and X = 1.0 in the steady state, in Tables 1, 2 respectively, and are found to be in good agreement.

Table 1 Comparison of local skin friction values at X = 1.0 and m = 0.5 with those of Hossain-Paul [9] for steady state purely fluid (Da $\to \infty$ in present model) case.

Pr	Hossain and Paul [9] $\Gamma_X/Gr_L^{3/5}$	Present results
0.01	5.13457	5.13424
0.05	2.93993	2.93180
0.1	2.29051	2.29044

Table 2 Comparison of local Nusselt number values at X = 1.0 and m = 0.5 with those of Hossain-Paul [9] for steady state purely fluid (Da $\rightarrow \infty$ in present model) case.

Pr	Hossain and Paul [9] $Nu_X/Gr_L^{3/5}$	Present results
0.01	0.14633	0.14648
0.05	0.26212	0.26227
0.1	0.33174	0.33648

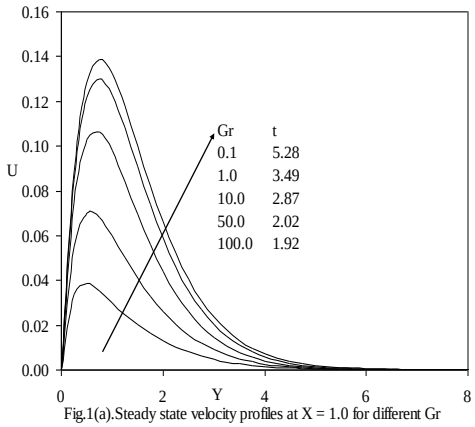

Fig.1(a).Steady state velocity profiles at X = 1.0 for different Gr

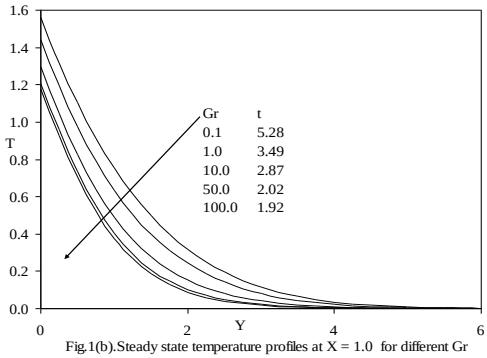

Fig.1(b).Steady state temperature profiles at X = 1.0 for different Gr

In **Figures 1(a) and 1(b)**, the influence of Grashof number (Gr_l) on steady state velocity(U) and temperature (T) distributions with Y-coordinate are shown. Free convection i.e. thermal buoyancy effects are analyzed via the Grashof number. For an increasing Gr_l from 0.1 through 1.0, 10.0, 50.0 to 100.0 cooling of the cone by free convection occurs i.e. heat is conducted away from the cone to the surrounding regime.

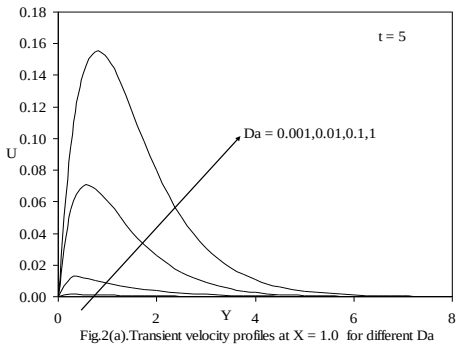

Fig.2(a).Transient velocity profiles at X = 1.0 for different Da

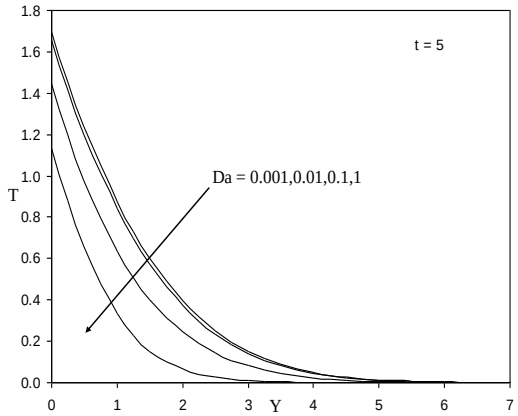

Fig.2(b).Transient temperature profiles at X = 1.0 for different Da

Figures 2(a) and 2(b) show the effect of Darcy number (Da) on dimensionless velocity (U) and temperature (T) with transformed radial coordinate (Y) close to the leading edge (i.e. cone apex) at X = 1.0. To study the influence of regime permeability from sparsely packed media to densely packed materials the following values Da = 1.0, 0.1, 0.01, 0.001 are considered. Da = K/L^2 for a fixed value of the reference length (L) is directly proportional to permeability (K) of the porous regime. Increasing Da increases the porous medium permeability and simultaneously decreases the Darcian impedance since progressively less solid fibers are present in the regime. The flow is therefore accelerated for higher Da values causing an increase in the velocity U as shown in Figure 2(a). Maximum effect of rising Darcy number is observed at intermediate distance from the cone surface around Y ~ 1. Conversely temperature T depicted in Figure 2(b) is opposed by increasing Darcy number.

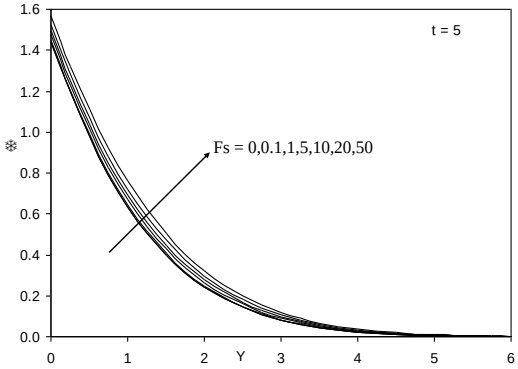

Fig.3.Transient temperature profiles at X = 1.0 for different Fs

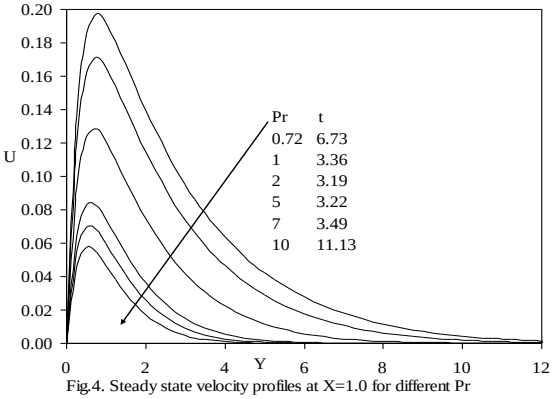

Fig.4. Steady state velocity profiles at X=1.0 for different Pr

The presence of fewer solid fibers in the regime with increasing Da inhibits the thermal conduction in the medium which reduces distribution of thermal energy. The regime is

therefore cooled when more fluid is present and T values in the thermal boundary layer are decreased. Profiles for both velocity and temperature are smoothly asymptotic decays to the free stream indicating that excellent convergence (and stability) is obtained with the numerical method. Velocity boundary layer thickness will be increased with a rise in Da and thermal boundary layer thickness reduced. The effect of the Forchheimer inertial drag parameter (Fs) on dimensionless temperature (T) profiles is shown in **Figure 3.** The Forchheimer drag force is a second order retarding force simulated in the momentum conservation equation. Increasing Fs values from 0.0 through 0.1,1.0,5.0,10.0,20.0 and 50.0 causes a strong increase in Forchheimer drag which decelerates the flow i.e. reduces velocities. For higher values of Fs it is expected that the porous medium flow becomes increasingly chaotic. Temperature (T) however is slightly increased with a rise in Forchheimer parameter. The effects of the Prandtl number (Pr) on velocity profiles are depicted in **Figure 4**. Pr encapsulates the ratio of momentum diffusivity to thermal diffusivity. Larger Pr values imply a thinner thermal boundary layer thickness and more uniform temperature distributions across the boundary layer. Hence thermal boundary layer will be much less thick than the hydrodynamic (translational velocity) boundary layer. Smaller Pr fluids have higher thermal conductivities, so that heat can diffuse away from the cone surface faster than for higher Pr fluids (thicker boundary layers). Physically the lower values of Pr correspond to liquid metals (Pr ~ 0.02, 0.05), Pr = 0.7 is accurate for air or hydrogen and Pr = 7.0 for water. The computations show that translational velocity U is therefore reduced as Pr rises from 0.72 through 1.0, 2.0, 5.0, 7.0 and 10.0 since the fluid is increasingly viscous as Pr rises. Figure 4(b) indicates that a rise in Pr substantially reduces the temperature T in saturated porous regime. The profiles become increasingly parabolic as Pr increases above 0.1, for which the profile is approximately a linear decay. For all cases T decays to zero as Y $\rightarrow \infty$, i.e. in the free stream. There is however a rapid decay to zero for the maximum Pr (= 10) where the temperature plummets to zero in the near-wall region. Concentration function values are seen to increase slightly with an increase in Pr.

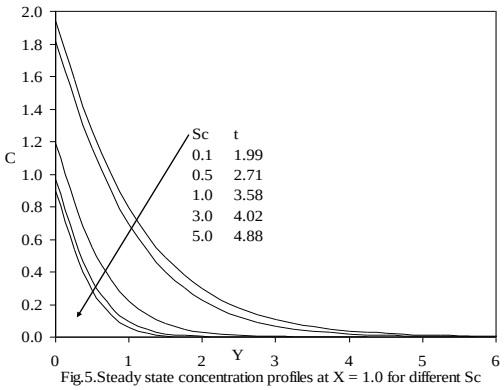

Fig.5.Steady state concentration profiles at X = 1.0 for different Sc

Figure 5 shows the effect of the Schmidt number (Sc) on the dimensionless concentration (C). We note that the Schmidt number (Sc) embodies the ratio of the momentum to the mass diffusivity. Sc therefore quantifies the relative effectiveness of momentum and mass transport by diffusion in the hydrodynamic (velocity) and concentration (species) boundary layers. Smaller Sc values can represent for example hydrogen gas as the species diffusing in air , Sc = 2.0 implies hydrocarbon diffusing in air, and higher values to petroleum derivatives diffusing in fluids (e.g. ethyl benzene) as indicated by Gebhart et al. [8]. As Sc increases, Figure 5 shows that C values are strongly decreased, as larger values of Sc correspond to a decrease in the chemical molecular diffusing i.e. less diffusion therefore takes place by mass transport. The dimensionless concentration profiles all decay from a maximum concentration to zero in the freestream. Greater Sc values correspond to lower chemical molecular diffusivity of the parent fluid so that less diffusion of the species occurs in the regime. Concentration boundary layer thickness will therefore be reduced. For low Sc fluid greater species diffusion occurs and concentration boundary layer thickness increased. For Sc = 1, the Concentration and velocity boundary layers will have approximately the same thickness i.e. species and momentum will be diffused at the same rates. With lower Sc values the decay of concentration from the cone surface is more controlled, for increasing values of Sc the profiles descend more and more steeply and concentration falls faster from the surface to a short distance into the boundary layer regime.

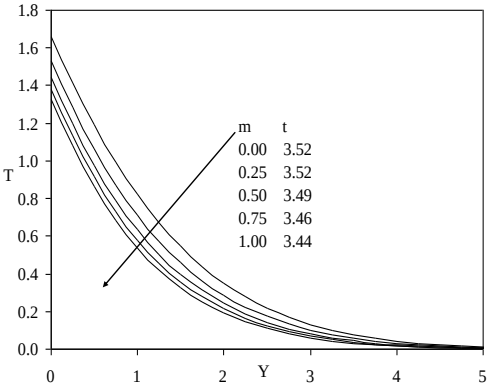

Fig.6.Steady state temperature profiles at X = 1.0 for different m

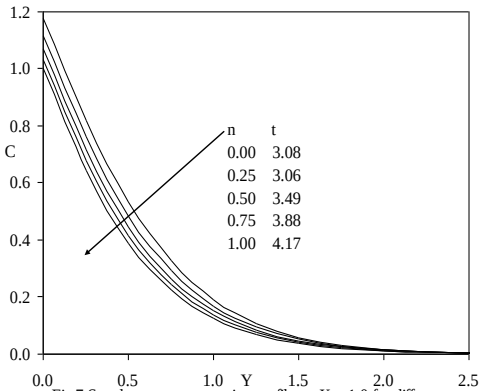

Fig.7.Steady state concentration profiles at X = 1.0 for different n

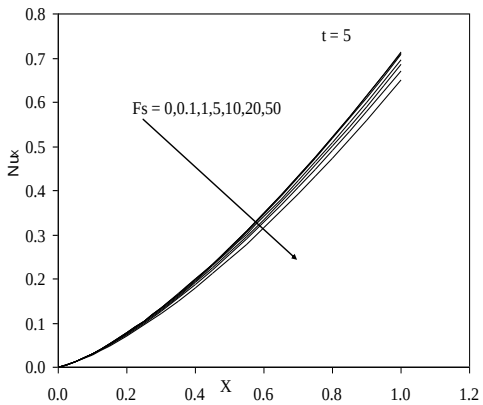

Fig.8.Effect of Fs on local Nusselt number at X = 1.0

The effect of surface heat flux power exponent (m) on the steady state temperature (T) is shown in **Figure 6**. An increase

in the value of m reduces the temperature. It is also seen that the time required to reach the steady state temperature is more at lower values of m. **Figure 7** depict the distribution of concentration (C) with radial coordinate (Y) for various values of the surface mass flux power law exponent (n). The concentration reduces with the increasing n values from 0.0 through 0.25, 0.50, 0.75 and 1.0. Increasing Fs clearly reduces the local Nusselt number as shown in **Figure 8**.

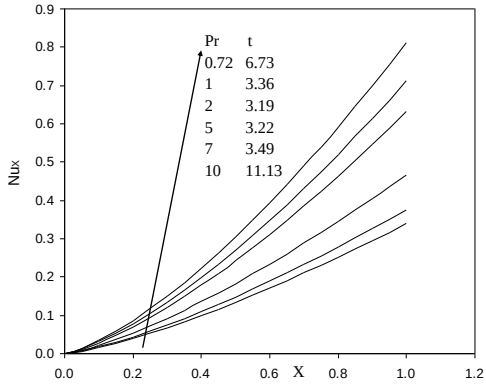

Fig.9.Effect of Pr on local Nusselt number at X = 1.0

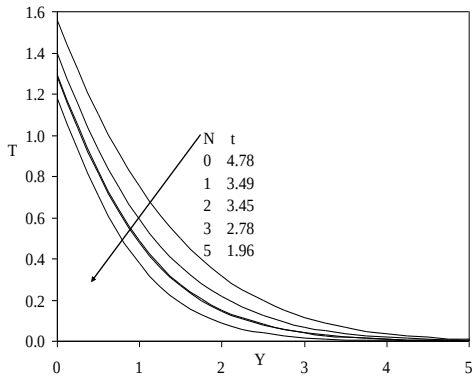

Fig.10.Steady state temperatue profies at X = 1.0 for different N

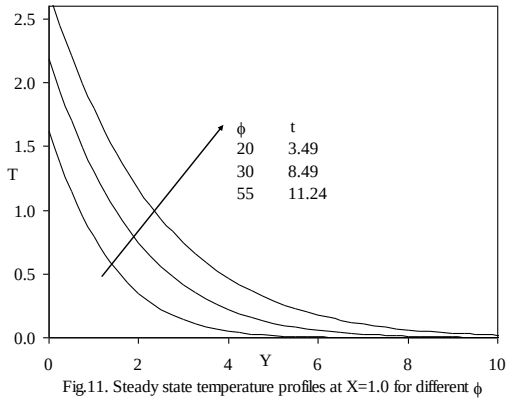

Fig.11. Steady state temperature profiles at X=1.0 for different ϕ

A slight increase in local Nusselt number accompanies the increment in Pr as shown in **Figure 9**. The influence of the concentration to thermal buoyancy ratio parameter (N), on dimensionless temperature (T) with radial coordinate (Y) is shown in **Figure 10**. N = 0 indicates that thermal and species buoyancy forces are both absent. For N > 0, thermal and species buoyancy forces aid each other. N = 1 implies that both buoyancy forces are of the same order of magnitude. A rise in N from 0.0 through 1.0, 2.0, 3.0 and 5.0 induces a retarding effect on the flow in the porous regime i.e. velocities are decreased. Increasing N (thermal and concentration buoyancy forces assisting each other) decreases temperatures in the regime i.e. cools the boundary layer regime. The effect of semi-vertical angle of the cone (ϕ) on dimensionless temperature (T) with Y-coordinate is shown in **Figure 11**.

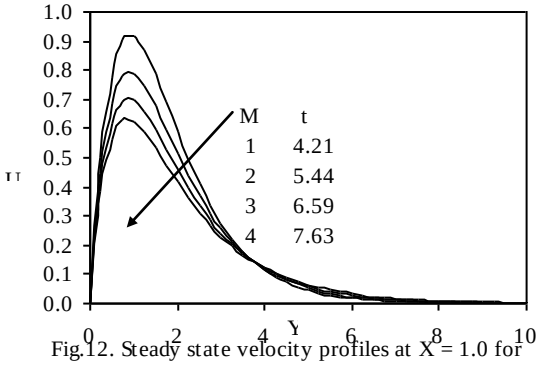

Fig.12. Steady state velocity profiles at X = 1.0 for different values of M

It is observed that a rise in ϕ substantially increases the temperature T in the boundary layer regime. And more time is required to reach the steady state. **Figures 12** the influence of magnetic parameter (M) versus spanwise spatial distributions of velocity U are depicted. Application of magnetic field normal to the flow of an electrically conducting fluid gives rise to a resistive force that acts in the direction opposite to that of the flow. This force is called the Lorentz force. This resistive force tends to slow down the motion of the fluid along the cone and causes an increase in its temperature and a decrease in velocity as M increases. An increase in M from 1 though 2, 3, 4 clearly reduces streamwise velocity U both in the near-wall regime and far-field regime of the boundary layer.

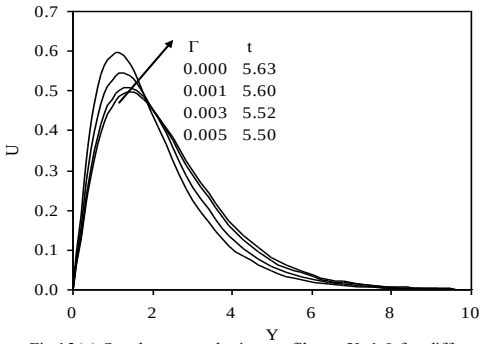

Fig.13(a).Steady state velocity profiles at X=1.0 for different Γ

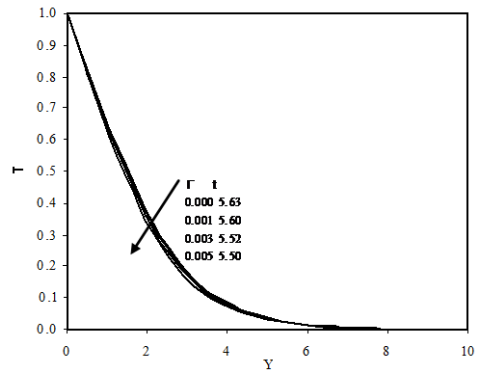

Fig.13(b).Steadystate temperature profiles at X=1.0 for different Γ

In **figures 13(a) to 13(c)**, we have presented the variation of streamwise velocity (*U*), temperature function (*T*) and concentration (*C*) versus spanwise coordinate (*Y*) with collective effects of viscoelasticity (Γ) and time (t), close to the leading edge (i.e. cone apex) at $X = 1.0$. An increase in Γ from 0 to

0.001, 0.003 and the maximum value of 0.005, as depicted in figure 1a, clearly enhances the streamwise velocity, U which ascends sharply and peaks in close vicinity to the cone surface ($Y = 0$).

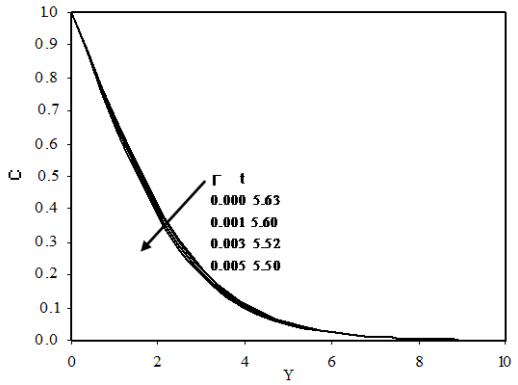

Fig.5.1(c).Steady state concentration profiles at X=1.0 for different Γ

In figure 1b increasing viscoelasticity Γ is seen to decrease temperature throughout the boundary layer. The graphs show therefore that increasing viscoelasticity cools the flow. With progression of time, however the temperature, T is consistently enhanced i.e. the fluid is heated as time progresses. A similar response is observed for the concentration field, C, in figure 1c. Increasing viscoelasticity again reduces concentration, showing that species diffuses more effectively in Newtonian fluids (Γ=0) than in strongly viscoelastic fluids. Once again with greater elapse in time the concentration values are reduced throughout the boundary layer regime ($0 < Y < 10$).

Conclusions

Numerical solutions have been presented for the buoyancy-driven unsteady natural convection boundary layer flow past a vertical cone embedded in a non Darcian isotropic porous regime. Present results are compared with those of Hossain and Paul [9] and found to be in excellent agreement. The following conclusions are drawn.

- Increasing viscoelasticity accelerates the streamwise velocity and enhances shear stress (local skin friction), local Nusselt number and local Sherwood number, but reduces temperature and concentration values transverse to the cone surface (i.e. inside the boundary layer regime).
- Increasing Grashof number boosts the translational velocity in the cone surface regime and decreases temperature throughout the flow regime.
- Increasing Darcy number accelerates the flow i.e. increases translational velocities. However the temperature is reduced with a rise in Darcy number.
- An increase in the Forchheimer inertial drag parameter is observed to slightly increase the temperature, but reduces both velocity and local Nusselt number.
- An increase in Prandtl number is observed to decrease both temperature and velocity, but the concentration is slightly increased. A slight increase in local Nusselt number accompanies the increment in Pr.
- The concentration is observed to significantly decrease with an increase in Schmidt number.
- The temperature is observed to decrease with an increase in buoyancy ratio parameter, but decrease with an increase in semi-vertical angle of the cone. The time taken to reach the steady state increases with increasing ϕ.

Nomenclature

x, y coordinates along the cone generator and normal to the generator
u,v velocity components along the x- and y-directions
g gravitational acceleration
r local radius of cone
t' time
t dimensionless time
T' temperature
T dimensionless temperature
C' concentration
C dimensionless concentration
D mass diffusion coefficient
K permeability of porous medium
q_w heat flux (i.e. heat transfer rate per unit area)
q_w^* mass flux (i.e. mass transfer rate per unit area)
k thermal conductivity of fluid
L reference length
X, Y dimensionless coordinates along the cone generator and normal to the generator
U,V dimensionless velocity components along the X- and Y-directions
b Forchheimer geometrical constant
Da Darcy number
Fs Forchheimer number
Gr_L Grashof number
M magnetic parameter
B_0 magnetic field strength
Pr Prandtl number
N buoyancy ratio parameter
Sc Schmidt number
k_0 Walters-B viscoelasticity parameter
Γ dimensionless Walters-B viscoelasticity parameter
m power-law index for surface heat flux relation
n power-law index for surface mass flux relation
Nu_x local Nusselt number
Nu_X dimensionless local Nusselt number
Sh_x local Sherwood number
Sh_X non-dimensional local Sherwood number
R dimensionless local radius of cone

Greek symbols

μ dynamic viscosity of fluid
ν kinematic viscosity of fluid
ϕ semi-vertical cone angle
α thermal diffusivity
β volumetric thermal expansion coefficient
θ dimensionless temperature function
τ dimensionless time
τ_X dimensionless local shear stress function (skin friction)

Subscripts

w condition on the wall
∞ free stream condition

References

[1] Bapuji Pullepu, Ekambavanan K, Chamkha AJ. Unsteady laminar free convection from a vertical cone with uniform surface heat flux, Nonlinear Analysis: Modelling and Control. 2008; 13: 47-60.

[2] Carnahan B, Luther HA, Wilkes JO. Applied Numerical Methods, John Wiley and Sons, New York; 1969.
[3] Chamkha AJ, Khalid ARA, Al-Hawaj O. Simultaneous Heat and Mass Transfer by Natural Convection from a Cone and a Wedge in Porous Media, J. Porous Media, 2000; 3: 155-164.
[4] Chen CH, Chen CK. Non-Darcian mixed convection along a vertical plate embedded in a porous medium, Applied Mathematical Modelling. 1990; 14: 482-488.
[5] Chen CK, Chen CH, Minkowycz WJ, Gill US. Non-Darcian effects on mixed convection about a vertical cylinder embedded in a saturated porous medium, Int. J. Heat Mass Transfer. 1992; 35: 3041-3046.
[6] Gouse Mohiddin S. Computational Fluid Dynamics, LAP Lambert Academic Publishing, Germany; 2011.
[7] Gouse Mohiddin S, Prasad VR, Varma SVK, Anwar Bég O. Numerical Study Of Unsteady Free Convective Heat And Mass Transfer In A Walters-B Viscoelastic Flow Along A Vertical Cone, Int J of Appl Math and Mech. 2010; 6: 88-114.
[8] Gebhart B, Jaluria Y, Mahajan RL, Sammakia B. Buoyancy – Induced flows and Transport, Hemisphere, New York; 1998.
[9] Hossain MA, Paul SC. Free convection from a vertical permeable circular cone with non-uniform surface heat flux, Heat Mass Transfer. 2001; 37: 167-173.
[10] Hossain MA, Paul SC. Free convection from a vertical permeable cone with non-uniform surface temperature, Acta Mechanica. 2001; 151: 103-114.
[11] Ingham DB, Pop I. Transport Phenomena in Porous Media II, Pergamon, Oxford ; 2002.
[12] Muthucumaraswamy R, Ganesan P. Unsteady flow past an impulsively started vertical plate with heat and mass transfer, Heat Mass Transf. 1998; 34: 187-193.
[13] Nield DA, Bejan A. Convection in Porous Media, 3rd edition, Springer, New York; 2006.
[14] Ramachandra Prasad V, Vasu B, Anwar beg O. Numerical modelling of transient dissipative radiation free convection heat and mass transfer from a non-isothermal cone with variable surface conditions. Elixir Appl Math. 2011; 41: 5592-5603
[15] Trevisan OV, Bejan A. Combined heat and mass transfer by natural convection in a porous medium, Adv. Heat Transfer. 1990; 20: 315-352.
[16] Vafai K, Tien CL. Boundary and inertia effects on flow and heat transfer in porous media, Int. J. Heat Mass Transfer. 1981; 24: 195-203.
[17] Vafai K (Ed.), Handbook of Porous Media, 2nd edition, CRC Press, Boca Raton 2005.
[18] Vajravelu K, Nayfeh L. Hydromagnetic convection at a cone and a wedge, Int Commun Heat Mass Transfer. 1992; 19: 701–710.
[19] Walters K, Non-Newtonian effects in some elastico-viscous liquids whose behaviour at small rates of shear is characterized by a general linear equation of state, Quart J Mech Applied Math, 15 (1962) 63.